Email: michel.tchilibou@legos.obs-mip.fr

Spectral Signatures of tropical Pacific dynamics from model and altimetry

M. Tchilibou[1], **L. Gourdeau**[1], R. Morrow[1], B. Djath[2], G. Serazin[1], Damien A.[1]

[1] LEGOS, UMR5566 CNRS-CNES-IRD-Université de Toulouse III, Toulouse, France ; [2] HZG Max-Planck-Straße, Geesthacht, Germany

1.Introduction

In addition to equatorial waves, the Pacific tropical ocean reveal the presence of meso and submesoscale energetic structures with a clear signature in vorticity (**Ubelmann et al., 2011**) (**Fig. 1**).

Yet the calculation of SSH spectral slopes from alongtrack altimetry, evaluated over the 250-70 km mesoscale range, are very flat in the tropics compared to mid latitudes (**Fig.2**).

This study revisits the Eddy Kinetic Energy (EKE) and SSH spectral signatures of the tropical dynamics, estimated from a model and altimetry. We analyze the global **1/12°, 5-day DRAKKAR model,** the regional **1/36°, 1-hr NEMO with/without tides**, **Jason and SARAL/AltiKa altimetric data**.

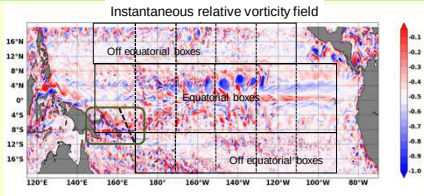

Fig. 1: DRAKKAR 1/12 relative vorticity snapshot. Black boxes are equatorial and tropical boxes analysed in the following. Green box: the domain of the 1/36° regional model. The dash line is the altimetric track to be compared with the regional model.

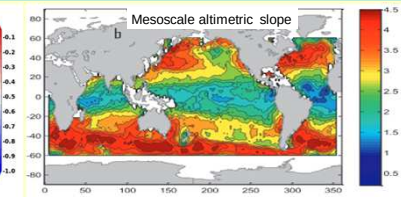

Fig. 2 : Altimery SSH spectral slope distribution from Xu and FU., 2012

2. Spectrum sensitivity to the preprocessing

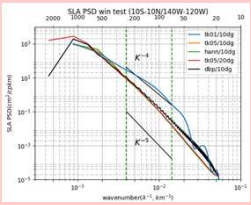

Fig. 3: SSH spectrum computed in equatorial boxes for 10° and 20° sizes using different spectral window .

After demeaning and detrending, we tested the sensibility of the spectra to the choice of spectral window and the data length.

Fig.3 shows the results for three spectral windows: **10 % cosine tapering (Tk01), tukey 0.5 (Tk05)** and **Hanning (Han)**. Over the 10° box at the equator, **Tk01** gives a relatively flat spectral slope. **We chose Tk05 since it preserves more of the original signal.**

At the equator, we recommend using 20° segments or square boxes to capture the SLA dynamics with spectral energy peaks reaching 700-1000 km wavelength. The inertial mesoscale range, with a k^{-5} slope extending to wavelength up to 700 km, is large compared to the standard range of 250-70 km (dashed green vertical lines) used to calculate spectral slope.

3. EKE/SLA frequency spectra

EKE (Fig. 4a): Most of the energy is concentrated in the equatorial belt. The maxima between 3°N-5°N corresponds with the 33-day **Tropical Instability Waves** (TIW) associated with unstable **Rossby waves**, and the 20-25 day equatorial TIW variability is associated with **Yanai waves [Farrar et al., 2008].** Centered at the equator, the 60-80 day variability is associated with **intraseasonal Kelvin waves** [**Cravatte et al., 2003**].
Poleward of 10°, **barotropic and baroclinic instabilities**, and nonlinear processes permit the appearance of energy at higher frequency than the critical frequency of the first mode baroclinic Rossby waves that varies from 60 days at 10°S to 110 days at 20°S (**Lin et al., 2008**).

SLA (Fig. 4b): SSH variability differs from the total EKE field with **a minimum of variability at high frequency along the equator** that highlights the significant ageostrophic component here, and zero Coriolis force.

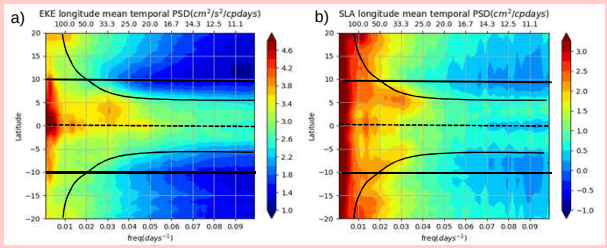

Fig. 4: Distribution in frequency of the zonal mean EKE (a) and SLA (b) energy as a function of latitude. The black curves represent the critical frequency of the first mode baroclinic Rossby waves.

4. Modelled SLA, EKE, Enstrophy wavenumber spectra

Energy and enstrophy 2-D spectra (**Fig. 5ab**) allow us to define **inertial ranges for the tropics**. For QG turbulence, the inertial range corresponds to the range with a conservation of energy and enstrophy. It is characterized by a KE spectrum that decreases steeply with wavenumber, and an enstrophy spectrum that is relatively flat (Richman et al., 2012). To identify the EKE redistribution within the inertial range, we calculated the kinetic energy flux π (**Fig. 5c**). Convergent π (negative slope) implies a kinetic energy sink over those length scales; positive slope implies a kinetic energy source around the wavenumber k_f defined by the point of the zero crossing (Sasaki and Klein, 2008; Scott and Wang, 2005).

Off the equator (red, green lines) the peak of enstrophy is at lower scale than the peak of energy in accordance with mid latitudes**, the inertial range extends from 300 km to 110 km**. π is negative, indicating **a dominant inverse cascade of energy** within the inertial range. A small direct cascade is present at smaller-scales.

In the equatorial belt, (**blue** line) energy and entrophy spectra peak at the same **570 km wavelength**, and the enstrophy spectra is relatively flat (k^{-1}) **down to 110 km delimiting the upper and lower bound of the inertial range** that is characterized by **a dominant direct cascade** as illustrated by positive π for scales up to 350 km.

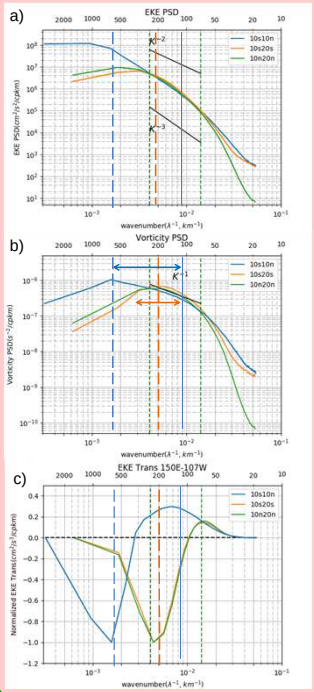

For geostrophically balanced flows, the SSH spectrum (**Fig. 5d)** should match the EKE spectrum multiplied by k^{-2}.

Off the equator, SSH (EKE) spectra exhibit a $k^{-4\ (-2)}$ slope within the inertial range, falling between the QG and SQG turbulence slope.

At the equator, the SSH spectral energy is weaker (see Fig. 4) than the total EKE including anisotropic flows. Over the 110-570 km inertial range, **SSH spectra exhibit a k^{-5} slope** in accordance with the k^{-3} slope of EKE spectra.

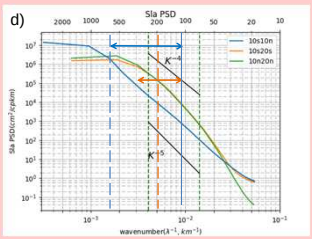

Fig. 5: a) Energy, b) Enstrophy, c) Energy flux, and d) SSH spectra for the 10°S-20°S and 10°N-20°N off equatorial areas, and the 10°S-10°N equatorial area. Arrows in 5b,d delineate off equatorial and equatorial tropical mesoscale range, based on the inertial range. Blue and orange dash lines are for the peak of energy and enstrophy . Black lines show specific spectral slopes. Green dash lines are for the standard 250-70 km mesoscale range.

5. Along track "altimetric" spectra

2-D spectra in section 4 are similar to 1-D meridional spectra, particularly in the inertial range (**Fig. 6**). 1-D meridional modelled SSH spectra are close to the orientation of along track altimetric spectra. At large scale both spectra compare well. In the inertial range **altimetric spectra is characterized by very flat slopes (k^{-1})** as in Xu and Fu (2012). In addition to altimetric noise, the flat slope in altimetric spectra may be **due to internal waves**, including baroclinic tides with a peak at 125 km (Dufau et al., 2016).

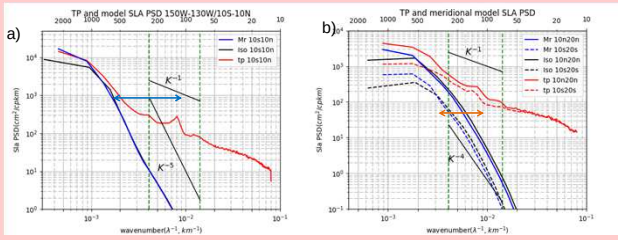

Fig. 6: 2-D (black), 1D Meridional modeled (blue) and along track altimetric (red) spectra for a) the equatorial Pacific, and b) the off equatorial Pacific. Arrows delineate off equatorial and equatorial tropical mesoscale range. Black strait lines show specific spectral slopes.

To highlight the **contamination of SSH spectra by baroclinic tides**, a 1/36° regional model of the South West Pacific with (**AM**)/without (**SM**) explicit tides was run (see **Fig. 1**). This area has a huge conversion of barotropic to baroclinic tides (Hiwa and Hibiwa, 2011). **1-D meridional SM** spectra based on 5-day output (**green**) are similar to the DRAKKAR output (**purple**) with a spectral slope from k^{-5} to k^{-4} (**Fig. 7**). The 1-hr SM output (**blue**) show the impact of high frequency signals.The major modification of the spectra is due to baroclinic tides with a slope that flattens to k^{-1} for **AM**. This last spectrum is very coherent with the **Jason-2 and Saral** altimetric spectra. Most of the variability in the inertial range is due to coherent baroclinic tides (**red**).

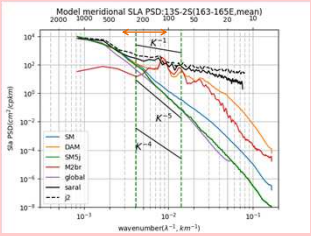

***Fig. 7:** In color, 1D Meridional spectra along the 13°-2°S section averaged between 165°-165°E based on 5-day outputs of the 1/12° global model (**purple**), on 5-day outputs of the 1/36° regional model without tides (**green**), on 1-hr outputs of the 1/36° regional model without tides (**blue**), and the 1-hr outputs of the 1/36° regional model with tides (**orange**). The spectra of the coherent baroclinic tides is in **red**. In **black**, altimetric spectra along the track shown on Fig. 1 based on Jason (**dash**) and SARAL/ALtiKa (**line**)*

Conclusion

SSH spectral shape and slope are sensitive to box and data size, particularly when using 10 % cosine tapering preprocessing, and a 10°x10° boxes in the equatorial Pacific. A Tukey 0.5 window is recommended in the tropics, and 20°x20° boxes are recommended at the equator.

The equatorial region (10S-10N) is dominated by long planetary waves and TIW/TIVs, and a mesoscale band ranging from 570 to 110 km. The off-equatorial region (poleward of 10°) reveals isotropic mesoscale signature within a 300-110 km mesoscale range caracterized by SSH/EKE spectra shapes falling betwwen QG and SQG turbulence.

The 250-70 km range classically used to estimate spectral slope to infer mesoscale dynamics is not well suited to the tropics where the mesoscale energy level is relatively low, and altimetric spectra are particularly impacted by tidal and internal wave signals.

Based on high resolution modeling with/without explicit tides, coherent internal tides are the main source to explain the flat slope of altimetric spectra which are polluted over a broad wavenumber range. Because of its better accuracy SARAL/AltiKA performs better than Jason.

References:
- Cravatte, S., J. Picaut, and G. Eldin (2003), Second and first baroclinic Kelvin modes in the equatorial Pacific at intraseasonal timescales, Journal of Geophysical Research-Oceans, 108(C8)
- Dufau, C., Orsztynowicz, M., Dibarboure, G., Morrow, R., and Le Traon, P.-Y.: Mesoscale resolution capability of altimetry: Present and future, J. Geophys. Res.-Oceans, 121, 4910–4927, doi:10.1002/2015JC010904, 2016.
- Farrar, J. T. (2008), Observations of the dispersion characteristics and meridional sea level structure of equatorial waves in the Pacific Ocean. J. Phys. Oceanogr., 38, 1669â€"1689.
- Lin X., J. Yang, D. Wu, and P. Zhai (2008), Explaining the global distribution of peak-spectrum variability of sea surface height, Geophys. Res. Letters., Vol. 35, L14602, doi:10.1029/2008GL034312.
- Niwa, Y., and T. Hibiya, 2011: Estimation of baroclinic tide energy available for deep ocean mixing based on three-dimensional global numerical simulations. *J. Oceanogr.*, **67**, 493–502, doi:10.1007/s10872-011-0052-1
- Richman, J. G., B. K. Arbic, J. F. Shriver, E. J. Metzger, and A. J. Wallcraft, 2012: Inferring dynamics from the wavenumber spectra of an eddying global ocean model with embedded tides. *J. Geophys. Res.*, **117**, C12012, doi:10.1029/2012JC008364.
- Sasaki H., and P. Klein (2012), SSH Wavenumber Spectra in the North Pacific from a High Resolution Realistic Simulation, J. Phys. Oceanogr., 42(7), 1233-1241.
- Scott, R. B. and F. Wang (2005), Direct evidence of an oceanic inverse kinetic energy cascade from satellite altimetry, J. Phys. Oceanogr., 35, 1650â€"1666.
- Ubelmann C. and L.L. Fu, (2011), Vorticity Structures in the Tropical Pacific from a Numerical Simulation, J. Phys. Oceanogr, 41, 1455-1464.
- Xu, Y., and L.-L. Fu, 2011: Global Variability of the Wavenumber Spectrum of Oceanic Mesoscale Turbulence. *J. Phys. Oceanogr.*, **41**, 802–809, doi:10.1175/2010JPO4558.1.